OFFICE OF NAVAL RESEARCH TECHNICAL REPORT FOR

**Molecular Dynamics Simulation of Interfacial
Electrochemical Processes: Electric Double Layer Screening**

Prepared for Publication for
ACS symposium Pacichem 1995
by
Michael R. Philpott
IBM Research Division, Almaden Research Center,
650 Harry Road, San Jose, CA 95120-6099
and
James N. Glosli
Lawrence Livermore National Laboratory,
University of California, Livermore, CA 94550

Abstract

The status of computer simulations of electric double layers is briefly summarized and a road map with bottle necks for solving the important problems in the atomic scale simulation of interfacial electrochemical processes is proposed. As an example of recent activity, efforts to simulate screening in electric double layers are described. Molecular dynamics simulations on systems about 4 nm thick, containing up to 1600 water molecules and NaCl at 1M to 3M concentrations, are shown to exhibit the main components of electric double layers at charged metal surfaces. Ion and water density profiles across the system show: a bulk electrolyte zone, a diffuse layer that screens the charge on the electrode and a layer of oriented water on the surface.

19960719 042

Molecular Dynamics Simulation of Interfacial Electrochemical Processes: Electric Double Layer Screening

Michael R. Philpott[1] and James N. Glosli[2]

[1]IBM Research Division, Almaden Research Center,
650 Harry Road, San Jose, CA 95120-6099
[2]Lawrence Livermore National Laboratory,
University of California, Livermore, CA 94551-9900

The status of computer simulations of electric double layers is briefly summarized and a road map with bottle necks for solving the important problems in the atomic scale simulation of interfacial electrochemical processes is proposed. As an example of recent activity, efforts to simulate screening in electric double layers are described. Molecular dynamics simulations on systems about 4 nm thick, containing up to 1600 water molecules and NaCl at 1M to 3M concentrations, are shown to exhibit the main components of electric double layers at charged metal surfaces. Ion and water density profiles across the system show: a bulk electrolyte zone, a diffuse layer that screens the charge on the electrode and a layer of oriented water on the surface.

This paper describes the application of molecular dynamics to chemical processes at the interface between a charged metal electrode and aqueous electrolyte. The long range goal is a scheme for the dynamics of chemical reactions on surfaces important in the electrochemical technology of power sources, electroplating, and corrosion control. The paper begins with a summary of our view of the current state of computer simulation applied to interfacial electrochemistry. Next we outline a map on which we plot a rudimentary road towards the goal. The status and road map are accompanied with a commentary on critical problems and potential bottle necks. To illustrate progress in the field we describe our simulations of screening of charged electrodes by aqueous electrolytes including previously unpublished work. Screening by double layers is an important physical phenomenon because double layers are some of the basic organizations adopted in electrochemical and biological systems to shield electric fields arising from layers or arrays of charge in contiguous structures. It is therefore important to understand their properties using models that can be solved without further approximations. The structure of the aqueous part of the double layer is given in terms of time independent water and ion probability distribution

functions averaged parallel to the metal surface. Electric fields and potentials are calculated from the microscopic charge density profile. These calculations provide a consistent microscopic picture of ions and water throughout a double layer including the species next to the charged surface (inner layer), in the 'diffuse layer' (also called the screening layer) and in the bulk zone. The effect of finite sized ions and water are clearly evident, as is the effect of the electric field on the orientation of surface water molecules.

Status of Molecular Dynamics Simulations

Figure 1 (top) is a sketch of the electric potential using Gouy-Chapman-Stern theory[1] in which the diffuse layer ions are treated as point charges, the water as a a dielectric continuum, and OHP and IHP (outer and inner Helmholtz planes) are introduced to mark the distance of closest approach of strongly hydrated ions and contact adsorbing ions respectively. molecules and ions for times as long as several nanoseconds. Research is not limited by computer power but by the availability of correct theories Figure 1 (bottom) shows a molecular scale cartoon of ions and water near a flat charged metal surface. Ideas embodied by pictures like this together with Gouy-Chapman-Stern theory and the thermodynamic theory of surface excess quantities have been used to analyze and interpret experimental electrochemical data[2-5]. The advent of risc based work stations allows the testing of atomic scale models of interfaces with hundreds and even thousands of molecules. Monte-Carlo and molecular dynamics computer simulations of ions and water molecules
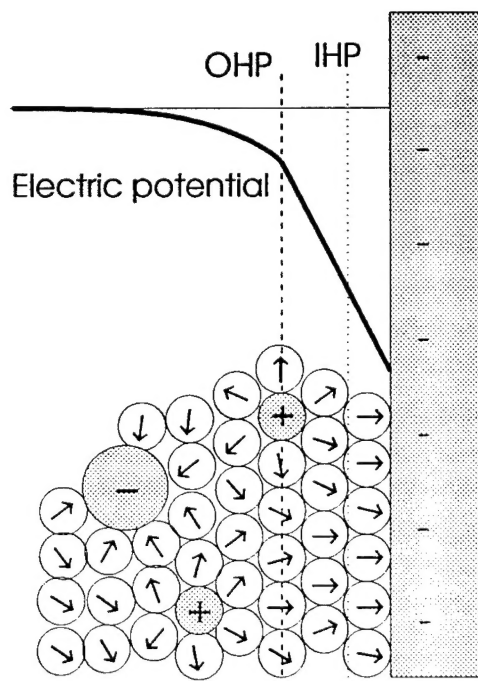
Figure 1. Schematic diagram (top) of electric potential across the double layer and (bottom) cartoon of the structure of water and ions next to a flat charged electrode.

interacting through various named potentials are routinely performed for a few thousand water of interfacial chemical processes and good algorithms for the efficient calculation of sums of long range electrostatic interactions. We comment first on electrostatics and boundary conditions, and then move on to other scientific issues.

Electrostatics. Three dimensional sums of electrostatic interactions (eg., ion-ion, dipole-dipole) are conditionally convergent. Available algorithms are getting faster and more useful all the time. However in studying the physics of electrified interfaces it is essential that the long range part of the electrostatic interaction be computed without truncation in a manner consistent with the boundary conditions. For example on a metal electrode Maxwell's equations connect electric field, potential with the total charge distribution (metal surface charge and charge on molecules and ions). For some geometries (eg., planar) the electric field of surface charge can be calculated by the method of images. In 3D systems if the electrostatic interaction is truncated the long range correlations responsible for dielectric polarization will be wrongly computed possibly causing like charged systems to attract. Parallel metal surfaces have an infinite set of multiple electrostatic images that have to be summed in plane-wise fashion to get the physics right[6, 7]. The crystal optics based methods of Ewald and Kornfeld are the simplest for calculating electrostatic fields[8]. The algorithm works for all space group symmetries. At best this method is order $N^{1.5}$ in the number of charges N. There are 2D summation methods that are faster[7, 9]. In our simulations we use the order N fast multipole method (fmm) developed by Greengard and Rokhlin [10-13]. It is a very useful method for large electrochemical simulations where a variety of boundary conditions (periodic, Dirichlet, Neumann or mixed boundaries) are encountered. It can also be adapted so that regions of low charge density are not subdivided when the charge count falls below a specified integer[12]. It is restricted to cubic shaped cells. The fmm is faster than Ewald for systems exceeding a few hundred charges[14]. Particle-mesh methods have been extensively used for long range r^{-1} potential problems[15]. For most systems P^3M is faster than fmm and can be used with orthorhombic simulation cells[16]. Recently we showed how to correctly calculate the fields from charge distributions. The effect of averaging over space regions spanning the size of a water molecule was explored[17, 18]. Though most experiments are done at constant potential, there are very few simulations at constant potential[19, 20].

Molecule-molecule and molecule-metal potentials. There are continuing improvements in molecule-molecule potentials. High quality efforts are directed at improving the interaction, including polarizabilies and getting away from vanilla Lennard-Jones forms[21, 22]. There are also potentials that include three body terms explicitly[23]. Possibly the best atom-metal potential is due to Barker[24]. The Barker potential for Xe/Pt(111) is an excellent fit to a large body of experimental data. There have been numerous quantum chemistry studies of ions and water on metal clusters some with applied fields and others on charged clusters to imitate the electrochemical environment (for water references see Zhu[25], for ions on clusters see Pacchioni[26]). Unfortunately only a few have been parameterized into pair forms useable in an MD code[25, 27-29]. For electrochemically interesting metals like Pt there are many compute intensive problems associated with cluster based po-

tentials of third row transition metals. Not the least are the relativistic orbital contractions and spin orbit effects. It would be better to focus on the sp metals like Cu or Ag. Even Au would be easier to work with than Pt since its d shell is more tightly bound. Recently several publications have reported cluster calculations for water and ions on Hg[30, 31] including a parameterization to give a pair potential for MD studies.

Dynamics. There are calculations in which the metal is modeled as an Einstein solid with harmonic vibrations[32]. When surface molecules and ions are strongly adsorbed molecular dynamics becomes an inefficient way to study surface processes due to the slow exchange between surface and solution. In this case it is possible to use umbrella sampling to compute distribution profiles[33, 34]. Recently the idea underlying Car-Parrinello was used for macroion dynamics[35, 36] in which the solvent surrounding charged macroions is treated as a continuum in a self consistent scheme for the potential controlling ion dynamics. Dynamical corrections from the solvent can be added. There is a need to develop statistical methods to treat the dynamics of complex objects that evolve on several different time scales.

Interfacial electron transfer. There have been several studies of electron transfer reactions[19, 37]and the connection with Marcus's theory[38]. It may be possible to use a Car-Parrinello like scheme on that part of the system directly affecting the electron transfer. There has also been very interesting studies of the ferro-ferri redox couple in solution[39, 40] that address many issues related to electron transfer from an electrode to a hydrated ion. Slow processes can be treated by transition state methods like the ones used in solid state ionic conductivity[41].

Ensembles. One goal of simulations is the calculation of experimental quantities. The most challenging are the Gibbs free energies of adsorption. Currently there is no proven scheme for constant chemical potential simulations of electrolyte adsorption on metals. It seems possible to develop Andersen's method[42] for (N,P,T) ensembles. Another possibility is an analog of the Gibbs ensemble[43] for electrolytes between plates with a bulk sample forming the second phase. In an interesting recent development the grand canonical Monte Carlo method was used for atomic fluid mixtures in a slit pore[44, 45].

Toward a Road Map

The intention is modest though the title of this section sounds pretentious. Given the current state of theory and simulation can we identify a path that will eventually lead to practical computation of reactions important to electrochemical technologies. To simplify the discussion we focus on technologies connected with: electric power sources, electroplating, and corrosion control. The key science problems are the following: deposition and dissolution of metal, formation of oxide layers, electron transfer from electrodes to ions, and charge migration in complex fluid phases. This is a broad range of processes. Let us first examine two existing methods: ab initio molecular dynamics and dynamics using potential energy surfaces.

Ab initio molecular dynamics. Chemical reactions involve the reorganization of electrons about the nucleii involved in the bond changes. The ab initio molecular dynamics scheme developed by Car and Parrinello[35] permits an accurate description of both electronic and nuclear rearrangements that occur during a reaction. The penalty for including electronic coordinates explicitly in an electrochemical simulation is the restriction to relatively few water molecules. Liquid water and proton transfer have been studied[46, 47]. The computational problem is immense so that at present the study of hundreds of water molecules takes too long. This number is quite enough for studying H-bonding and dissociation and the dynamics of the hydration of ions but is insufficient to deal with double layer structure or reactions of hydrated ions with charged metals.

Potential energy surfaces. For systems where some or all of the dynamics can be described by a potential energy surface (PES) it is possible to avoid solving the electronic Schrodinger equation, and use instead a PES parameterized with experimental data. Several cases already exist. First there is the well known S_N2 reaction

$$Cl^- + H_3C - Cl \rightarrow Cl - CH_3 + Cl^-. \qquad [1]$$
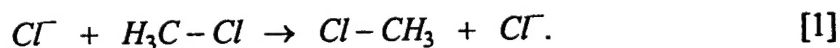
The molecular dynamics of this reaction has been studied in the gas and solution phases. Another example is the Brenner bond order potential[48]. used to describe the dynamics of homolytic bond fission and formation in carbon and hydrogen containing systems. These examples involve the making or breaking of two electron bonds between low Z atoms. Explicit degrees of freedom for the electrons are avoided though the use of a PES. The electrochemical problems are harder. They involve charged metal surfaces, charge transfer in polar environment and dynamics on several time scales. In surface UHV adsorbate studies considerable progress has been made understanding chemical dissociation reactions and physical sputtering using a combination of LEPS potential for the diatomic on the metal with a many body embedded atom potential for the metal.

Road map. Consider first the deposition and dissolution of metal ions on charged surfaces. If systems can be identified where adiabatic potentials could be used to describe the nuclear motion then by analogy with the experience gained with the dissociation of diatomics on metal surfaces[49] and with carbon-hydrogen chemistry[50] it should be possible to describe how metal ions adsorb on metals and conversely how metals dissolve. Once this is achieved it should be possible to formulate schemes to describe the formation of insoluble metal oxide layers. This would also require a model for water decomposition on metals. The central force model which permits water dissociation[51, 52] would have to be developed for the surface environment. The third process involves understanding how electrons cross from a metal to ions or organic molecules and initiate chemical reactions. It is possible that some of these reactions could be studied by treating the electron quantum mechanically moving in a potential defined by classical mechanics motion of molecules and ions in the double layer. Solvated electrons in liquids are studied this way. If not then hybrid Car-Parrinello schemes would have to be developed. The fourth class we have picked is important for ion mobilities in lithium ion batteries. It may be

possible to study these systems using ideas borrowed from small polaron motion in solids, using transition state dynamic methods of Bennett[41], or using recent theories of macroion motions[36]. Though we are presently a long way from providing technologically useful information, we believe that being able to model aspects of these processes would provide atomic scale insight as to how these technologies work.

Details of the Model

Screening is treated using the immersed electrode model[14, 53, 54]. A layer of electrolyte with an excess of positive ions is confined by a semi-infinite metal on the rhs and a restraining non-metallic wall on the lhs. There is no external electric field. The metal is grounded to zero electric potential. The charge on the electrode equals the image charge of the excess positive ions (-4e or -8e) so that the metal charge is completely screened by the ions in solution. The difference between these and earlier simulations [14, 53-56] is size, here there are enough ions and water to form a bulk electrolyte region where the solution is locally neutral. Because there is only one metal surface (shown on the rhs in all the figures) there are no multiple electrostatic images in the direction perpendicular to the metal[6, 7]. The electric field and potentials are calculated using previously developed methods[17, 18].

This work uses the SPCE water model[57] (three charged mass points, $q_H =$ 0.4238e, bond angle 109.5°, OH bond length 0.1 nm, Lennard-Jones sphere with radius $\sigma = 0.317$ nm and well depth $\varepsilon = 0.650$ kJ/mole) and associated parameters for NaCl[58]. The coordinate origin is at the center of the cell, and the axes are perpendicular (z) and parallel (x,y) to the metal surface. The simulation cell has edge length L=3.724 nm, the flat metal plane is at $z = 1.862$ nm and the flat restraining wall at $z = -1.862$ nm. The cell contains upto 1600 water molecules and the ion concentrations are approximately 1M, 2M or 3M NaCl. The metal charge density is either -0.046 Cm^{-2} (-4eL^{-2}) or -0.092 Cm^{-2} (-8eL^{-2}). Contact adsorption of ions is minimized. The cation has a smaller radius than the anion, so its hydration shell is strongly bound making it difficult for it to contact adsorb. The negative metal charge makes it energetically unfavorable for the anions Cl⁻ to contact adsorb.

Two potentials are used to describe the interaction of water and ions with the metal. A 9-3 potential is used to for the Pauli repulsion and the attractive dispersive interactions between molecules or ions and the metal. The interaction between a charge on an ion or water with the conduction electrons of the metal is modeled with a classical electrostatic image potential. The position of image plane and origin plane (same as the plane through nuclei of the surface) of the 9-3 potential was taken to be coincident. In real materials the image and nuclear planes are not coincident. This is not important in the simulations because the thickness of the repulsive wall is large (ca. 0.247 nm). The 9-3 atom-surface wall parameters describing interaction with nonconduction electrons were chosen to be the same as that used by Lee etal[59], A=17.447x10^{-6} kJ(nm)^6/mole and B=76.144x10^{-3} kJ(nm)^3/mole for the O atom. The A and B parameters for H were set to zero. The potential corresponding to these parameters describe a graphite-like surface. A useful reference point in the wall potential is at z_w=1.615 nm where the 9-3 wall potential changes sign. Each

simulation was run for about a nanosecond, and the instantaneous positions of all the atoms recorded every picosecond. The first 100 ps were discarded as anneal time. The density probability functions $\rho(z)$ were constructed by binning the configurations in bins (width L/800) parallel to the metal surface to give functions of z only.

## Screening of Charged Metal Electrodes in SPCE Electrolyte

We begin with remarks on the screening of charged surfaces by aqueous electrolytes. At high salt concentrations the region with excess ionic charge is microscopically small. A rough estimate of the thickness of the zone in which screening occurs, valid for dilute solutions (< 0.1M), is given by the inverse of the Debye-Hückel screening constant[60]

$$d = \sqrt{\left(\varepsilon kT/(8\pi e^2 n_b v^2)\right)} . \qquad [2]$$

Here ε is the macroscopic dielectric constant of the solvent (ca. 80 for water), v the valence of the ion (one in this paper), and n_b is the bulk concentration of the ions. Typical values of d are: 3 nm in 0.01M, 1 nm in 0.1M, 0.3 nm in 1.0M, and 0.2 nm in 3M NaCl solutions. Obviously in high salt concentrations the screening should be more efficient and the screening length smaller, but since the number for 1M NaCl is the diameter of a water molecule, and the number for 3M NaCl is even smaller, these numbers mean nothing without some additional atomic scale in sight like that provided by MD simulations. At high concentrations there are many problems with simple Gouy-Chapman theory[61-63] and many modifications have been proposed[60]. There are three main problems: the dielectric constant of water in a high surface field, the lower length scale due to the finite molecular size, and correlated motion amongst ions and water. For example there is no reason to believe that the value of ε is 80 near a surface or in a field high enough for dielectric saturation to occur. This aspect has been discussed many times in the electrochemical literature[64]. Though we take the Debye length for concentrated solutions as an rough measure of double layer thickness, we should be very cautious when d approaches the size of a water molecule.

Figure 2 shows the distribution of the ions for three separate calculations with concentrations 1M, 2M and 3M NaCl. The charge on the electrode was -4e for 1M and 2M and -8e for 3M. The temperature was 30°C for 1M and 2M, and 100°C for the 3M NaCl solution. Note that there is no significant contact adsorption. All the peaks in the ion distributions occur away from the position of closest approach $z_w=1.612$ nm to the metal. This is precisely the situation we contrived for the reasons given before. The ion concentrations are approximately the same for $|z| < 1.0$ nm. This identifies the region of the system with bulk electrolyte properties. For $|z| < 0.5$ nm the two ion profiles are the same within 10 to 20%, for all the simulations. The bulk region is smaller for 1M NaCl because the screening layer is thicker. The integrated ion densities are monotonically increasing curves in Figure 2. They provide a rough measure of overall charge neutrality from the restraining wall to the metal. The vertical arrows indicate roughly where the ion charge densities start to diverge because of screening. Also shown in Figure 2 are the results of a calculation of ion
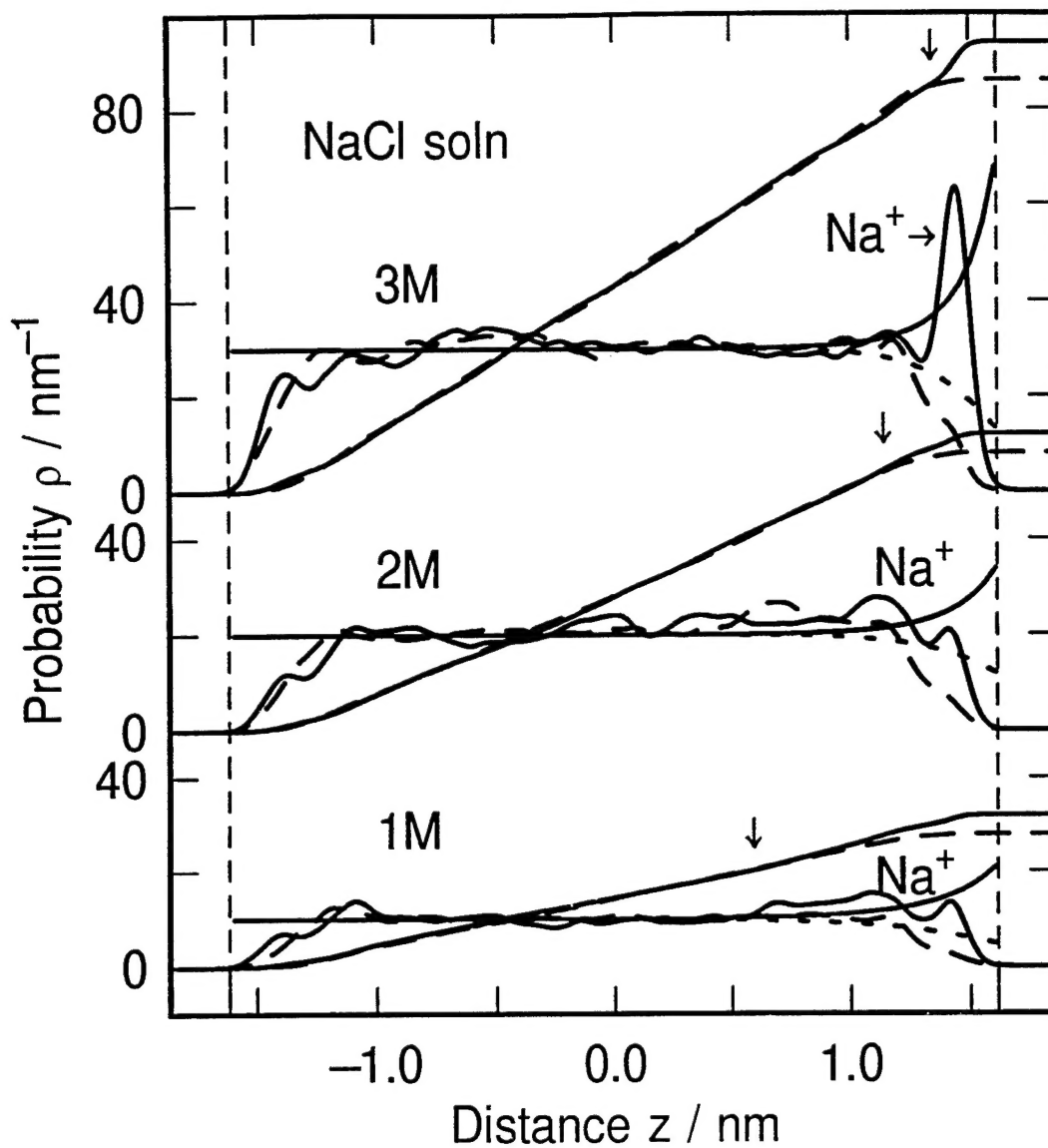
Figure 2. Ion probability density distribution profiles for NaCl solution. 1M and 2M solution at 30°C and -4e electrode charge, 3M solution at 100°C and -8e electrode charge. Also shown: integrated ion densities and Gouy-Chapman ion densities.

densities using simple Gouy-Chapman theory. For optimal comparison the electrode was assume to start at z=1.612 nm. These superimposed curves show how lack of atomic scale structure limits the application of Gouy-Chapman theory. This is graphic evidence that there are important details in MD simulations due to hydration, molecular size, and water layering near charged surfaces.

In each case the width of the screening layer is too small to justify the description as 'diffuse' (though we will continue to use this term). To estimate the diffuse layer width we measure from the z=1.615 nm (where wall potential changes sign) to the point where the difference in integrated ion densities is e^{-1} of the metal charge (8e for 3M, 4e for 1M and 2M). For the solutions we find: 0.5 nm (0.31 nm)

for 1M, 0.4 nm (0.24 nm) for 2M, 0.2 nm (0.18 nm) for 3M. The Debye shielding lengths calculated using Eqn(2) are in parentheses. Made with these favorable assumptions the agreement is remarkably close. It could be changed immediately if we used $\varepsilon = 6$, a value more appropriate for a zone in which the dielectric properties of water are at saturation values[64].

Looking at the fine structure in the density profiles we see that on the metal side all the chloride distributions have weak features at ca. 1.2 nm and 1.4 nm. Both appear to be associated with peaks in the cation distribution and may therefore be due to contact pairs or solvent separated pairs. Of course the SPCE model for water was not designed with high salt concentrations in mind, so the ion pairs may be more a feature of the model and not nature. Correlation between ions at high salt concentrations alter the distribution near the charged surface. Note that there is no association of oppositely charged ion peaks at the left wall in Figure 2.
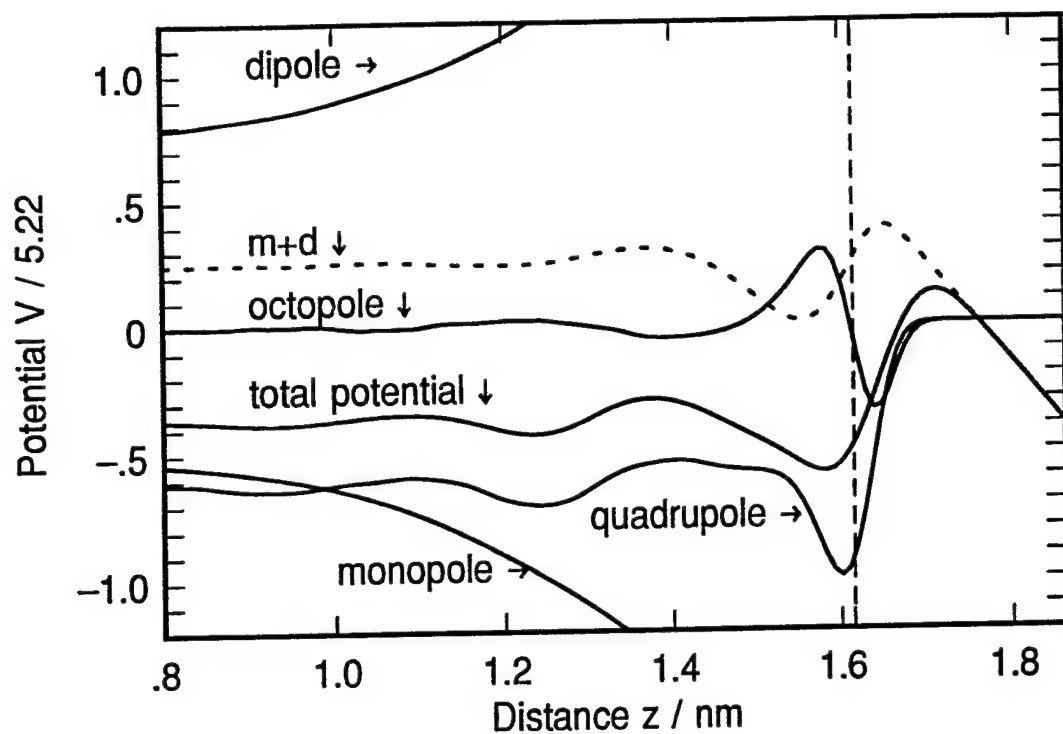
1M NaCl Solution

Figures 3, 4 and 5 show the results of an MD simulation using 1M NaCl solution. In this simulation the cell contains 32 Na^+ ions, 28 Cl^- ions, and 1576 water molecules at 30°C. The electrostatic charge on the electrode surface due to the difference in number of positive over negative ions is $-4|e|$ or -0.046 Cm^{-2}. The top panel in Figure 3 shows the probability density profiles for the water proton, water mass center, Na^+ ions and Cl^- ions. Both ion distributions have been smoothed to permit clearer identification of variations in density with position. We saw in Figure 2 the near coincidence of the integrals of the ion density for $z < 0.7$ nm which shows that the electrolyte is approximately charge neutral before this point. For $z > 0.7$ nm the integrated densities systematically diverge as expected for a transition from the locally neutral 'bulk' electrolyte into the 'diffuse' part of the electric double layer. The Na^+ ion distribution shows well defined structure in the form of a broad peak at ca. 1.1 nm, and a sharp peak at 1.4 nm. The water and proton distributions appear flat for $|z| < 0.8$ nm. On the metal side the water probability distribution has peaks at 0.9 nm, 1.2 nm, and a strong asymmetric peak at 1.6 nm. This latter feature appears to be composite being the superposition of a broad feature at 1.5 nm and a narrow peak at 1.6 nm. The peaks in the proton distribution are at 0.9 nm, 1.2 nm, 1.55 nm, and 1.7 nm. The last peak at ca. 1.7 nm comes from protons in water OH bonds pointing at the metal.

The bottom panel in Figure 3 shows the potential calculated using the atom method, and the components of the potential calculated by the molecule method[17, 18]. The contact potential is about -2V, and the potential in the 'bulk-like' zone comes from the water quadrupole. The monopole curve is from the ionic charge. If the system were truly neutral then the monopole curve would be flat and zero all the way to the beginning of the diffuse layer. The transition to monotonic decrease starting near $z = 0.7$ nm is another indicator of where the diffuse layer begins in this simulation. Note that combined monopole and dipole potential curve m+d shows that the dipole potential almost completely compensates the monopole. Adding the quadrupole to m+d shifts the core region downwards by 3V and brings the molecular calculation of potential into fair correspondence with the atom method
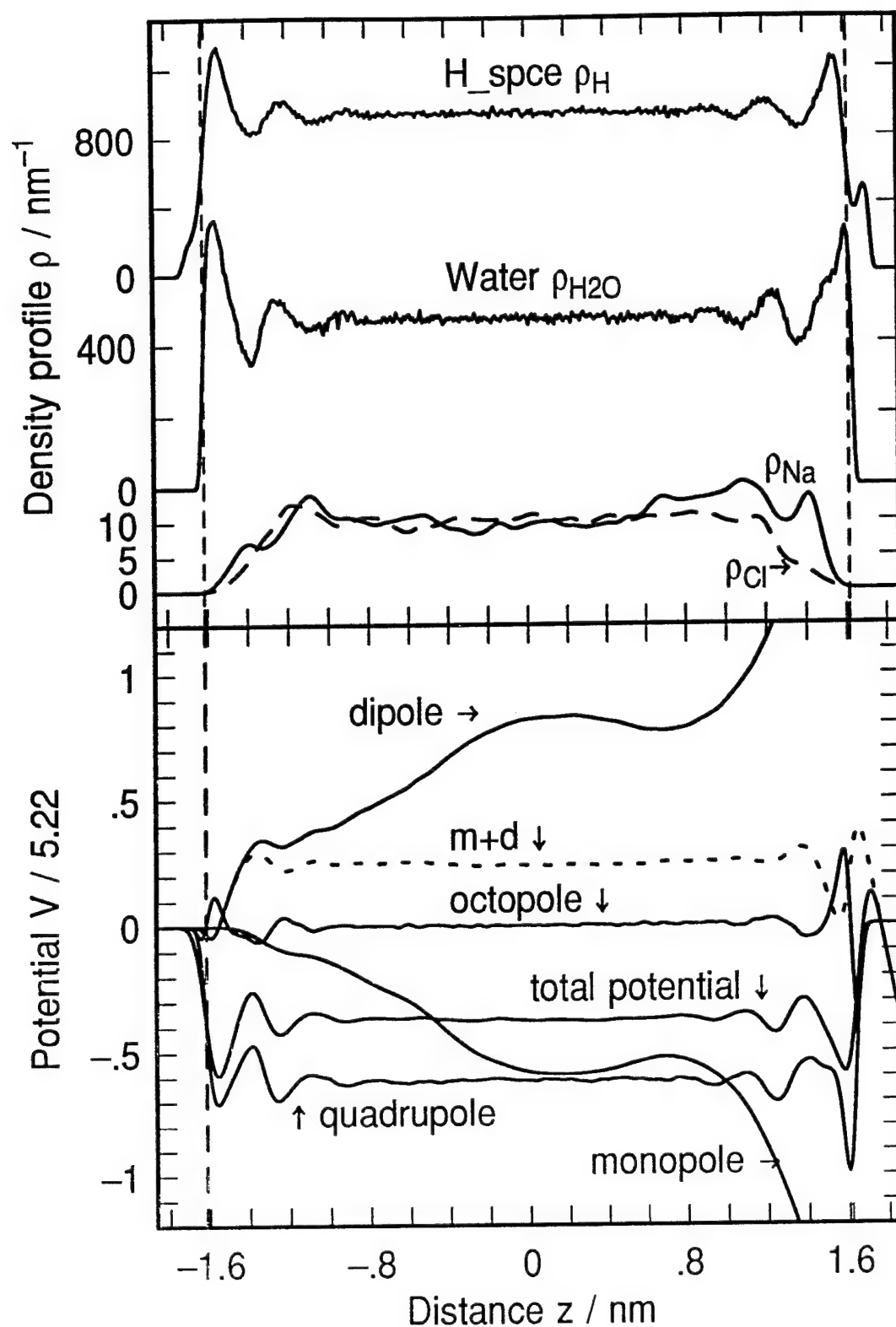
Figure 3. Top. Probability density distribution profiles for 1M NaCl solution at 30°C and -4e electrode charge. Bottom. Total electric potential and component multipole potentials. Total potential by atom method.

Figure 4. Detail of individual electric potentials for z > 0.8 nm.. 1M NaCl solution at 30°C and -4e electrode charge.
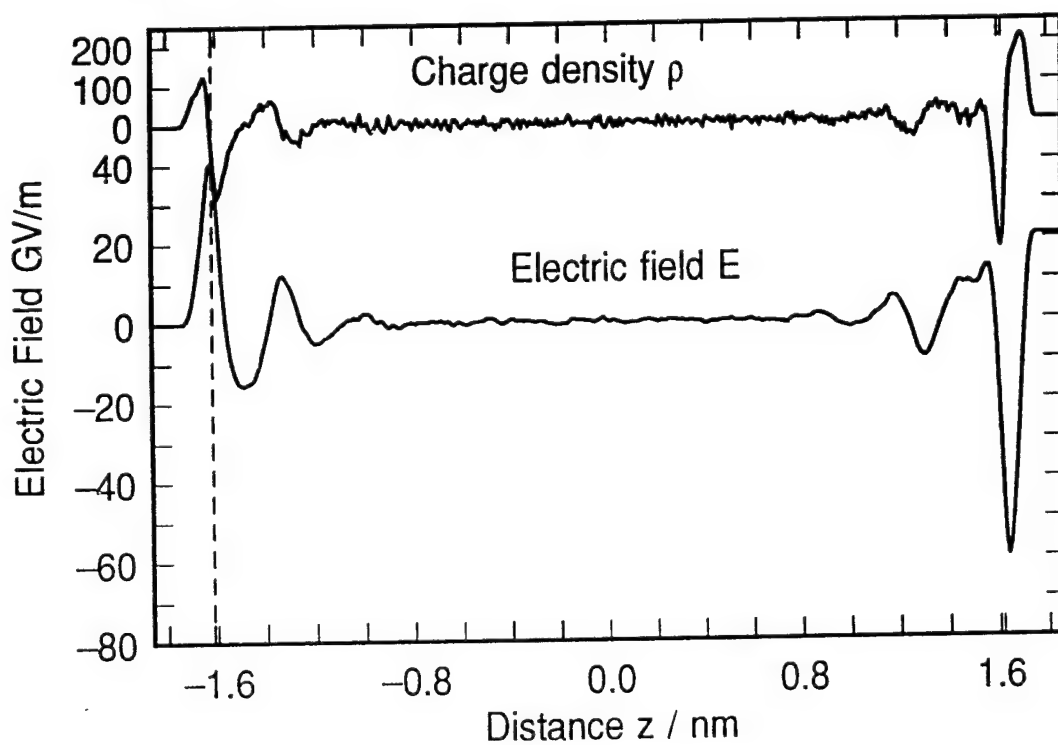
Figure 5. Microscopic electric charge density and electric field 1M NaCl solution.

of calculation. Adding the octopole improves the agreement at the walls. The molecular method has larger extrema near the surface compared to the atom method. The reason for this is the need to include many high order multipoles in the molecule method. However the contact potential is the same in each case since it depends only on m and d[65].

Figure 4 shows a detail of the the potentials shown in Figure 3 (bottom) for the region $z > 0.8$ nm. We note that the monopole and dipole determine the potential at contact. The quadrupole potential is very important in bulk and at the surface. The octopole potential is important near the surface. In the future as water models improve it will be very important to include these terms. Obviously the surface potential relative to bulk solution must include the quadrupole term. Figure 5 shows the atomic charge density and the electric field along the z axis. Note that the charge density appears flat for $|z| < 0.8$ nm. The contribution from the ionic charge for $z > 0.8$ nm is not evident because the charge on the water molecules dominates. The electric field was obtained by integration of the charge density from $-\infty$ to position z. The field is flat with small variations around zero in the region $|z| < 0.8$ nm. Near the metal the electric field undergoes a series of rapid oscillations due to the water packing structure at the interface. The small overall rise in field from bulk to surface is due to the excess Na^+ charge in the screening layer. The oscillation near $z = -1.615$ nm is due to layering at the restraining wall. This is an unwanted artifact of the immersed electrode model. It does not occur if the water density is decreased to the point that a vapor-liquid interface opens up at the restraining wall. Space prevents discussion of emersed electrodes[66, 67] which have a vapor-liquid interface[68-70] and a liquid-solid interface[71].

2M NaCl Solution

Figure 6 shows the results for a 2M NaCl solution at 30°C. There are 62 Na ions, 58 Cl ions and 1516 water molecules, the image charge on the electrode is $-4|e|$. The cation and anion concentrations are approximately the same for $|z| < 1.0$ nm. The bulk region appears larger than in 1M NaCl solution consistent with narrower screening zone. There are many similarities between Figures 3 and 6. The detailed proton and water profiles for $z > 1.4$ nm look the same. The bottom panel in Figure 6 shows the total potential calculated using the atom method, and the components of the potential calculated by the molecule method. The contact potential is about -2V, just the same as in the 1M case. The difference between 1M and 2M come mainly from the ion distributions and their direct interaction with the waters. Thus the monopole and dipole potentials are different, but since as already seen for 1M, they cancel each other, the main contribution to the total potential in the bulk region comes from the quadrupole. The water distributions for 1M and 2M are also similar and so are the potentials which come from water. Again if the system were truly neutral the monopole curve would be flat all the way to the edge of the diffuse layer. It is flatter than the 1M case and oscillates about zero before diving down to large negative values for $z > 1.2$ nm. A key observation is the dependence of m+d on position. In all the simulations the m+d potentials are similar even though m and d are not. The transition to monotonic decrease starts near $z = 1.2$ nm is another in-
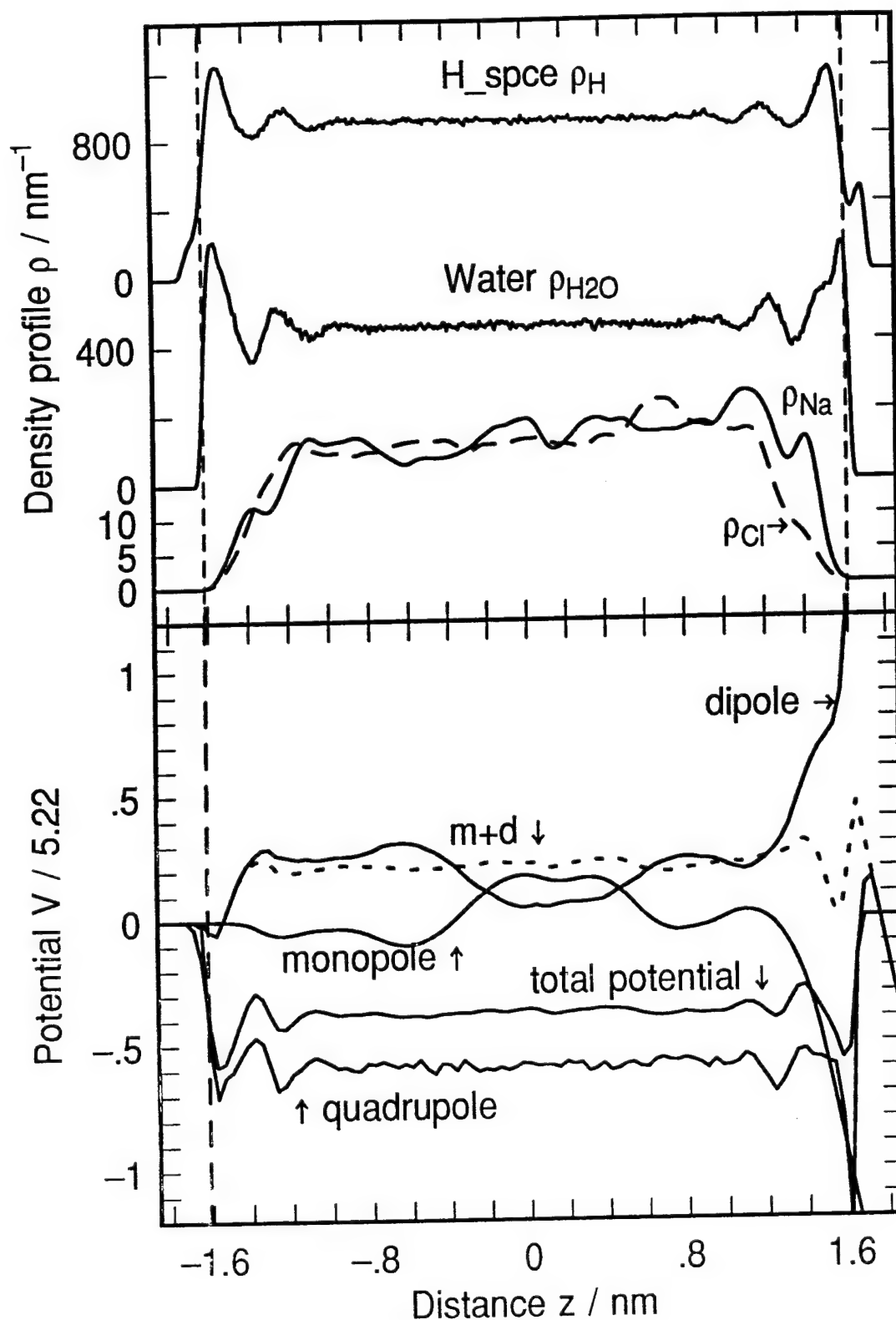
Figure 6. Top. Probability density distribution profiles for 2M NaCl solution at 30°C and -4e electrode charge. Bottom. Total electric potential and component multipole potentials. Total potential by atom method.

dicator of where the diffuse layer begins in this simulation. Including the quadrupole shifts the 'core' region down by -3V and brings the molecular calculation of potential into correspondence with the atom potential.

3M NaCl Solution

Figure 7 displays the results for 3M NaCl. There are 94 Na ions, 86 Cl ions and 1463 water molecules at 100°C, and the charge on the electrode is -8|e| or -0.092 Cm^{-2}. Calculations at high temperature were originally selected to improve the statistics. Subsequently the temperature dependence in the range 30 to 100°C was found to be weak. The Na^+ screening charge is concentrated in the peak at 1.45 nm less than one water diameter removed from where the 9-3 wall potential passes through zero (z_w = 1.615 nm). The peak in the cation distribution results from the strong primary hydration shell of the cation. The solvent layer at the electrode also effects the position and shape of the cation distribution near the metal. Note that for $|z| < 1.0$ nm the cation distribution is approximately flat at 30 ions nm^{-1}. There is also a small peak on the left hand side at ca. z = -1.4 nm, that is not associated with screening but is likely due to layering of the water molecules at the restraining wall. The chloride probability distribution has no major structural features, certainly none like the Na^+ screening peak at z = 1.45 nm. Starting from the metal on the right side of Figure 1, the chloride ion distribution rises to a plateau for $|z| < 1.00$ nm. The chloride and sodium ion probabilities are sufficiently similar across the plateau region for us to call this the bulk zone. This 3M NaCl simulation has the best statistics, as can be seen by the degree of local charge neutrality (ion densities are the same), and very nearly equal integrated densities shown in Figure 2.

The metal charge is twice that of 1M and 2M creating a stronger surface electric field, which results in more oriented waters in the first layer. The height of the proton peaks either side of the main water peak suggest that some H bonds to the bulk region are broken and that OH bonds point directly toward the metal. This electric field effect is distinct from localization of water on Pt(100) and Pt(111) surfaces in the simulations of Heinzinger and Spohr[27], and Berkowitz[28, 29]. In these papers water is localized on top sites of the Pt surface due to directed features in the chemisorptive potential.

The bottom panel of Figure 7 shows the potential calculated using the atom method, and some of the components of the potential calculated by the molecule method. The contact potential is larger due to higher electrode charge. Once again the importance of quadrupole terms is apparant. The m curve due to the ionic charge hovers around zero for z < 1.4 nm. The monopole potential is quite flat outside the screening layer. The transition to monotonic decrease starting near z = 1.4 nm is an indication of where the diffuse layer begins. Again m+d shows that the dipole potential completely compensates the monopole outside the screening zone. Including the quadrupole shifts the core region by -3V and brings the m+d potential into closer correspondence with the total potential calculated by the atom method.
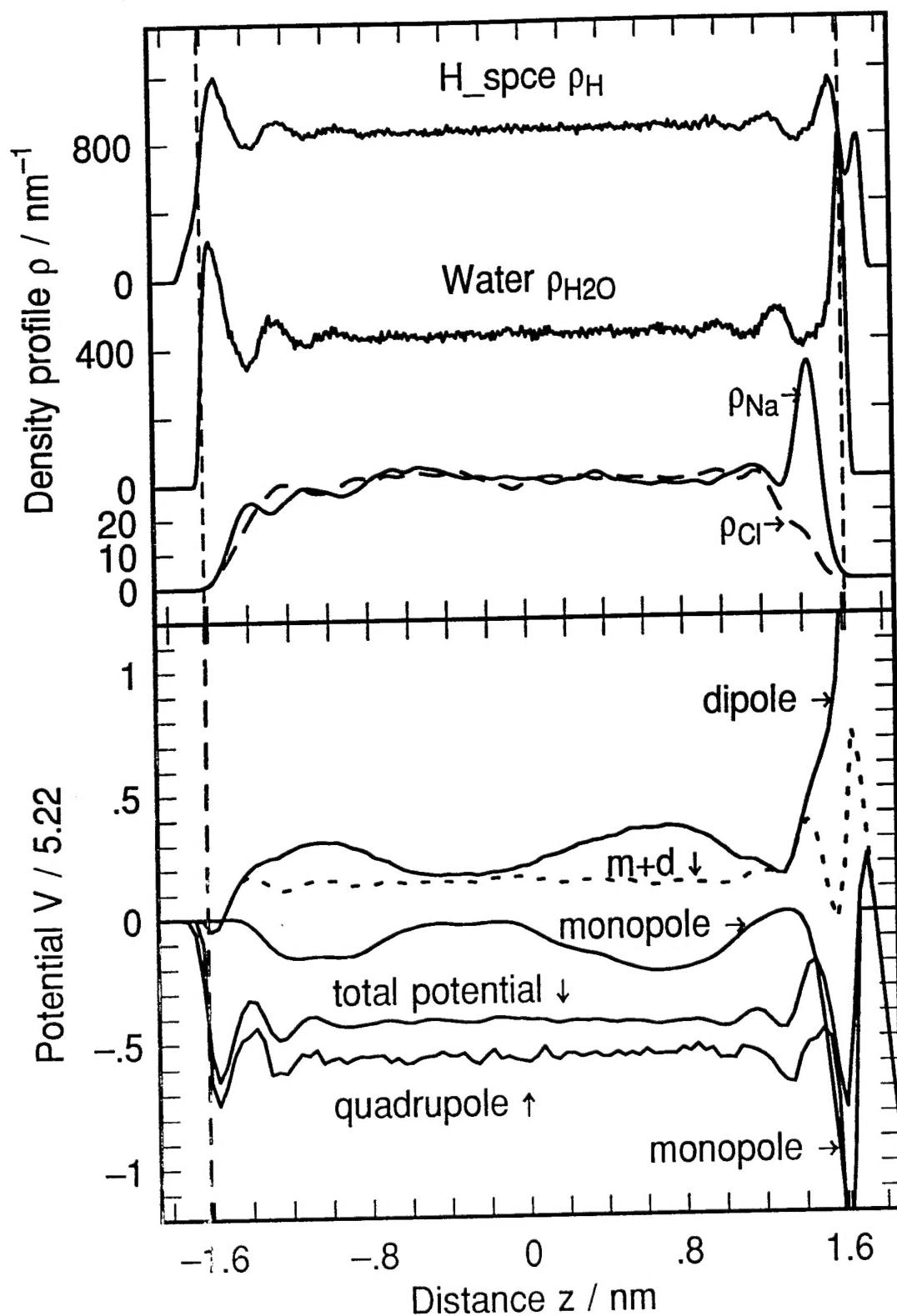
Figure 7. Top. Probability density distribution profiles. 3M NaCl solution at 100°C and -8e electrode charge. Bottom. Total electric potential and component multipole potentials. Total potential by atom method.

Conclusions

In this paper we briefly reviewed our view the status of MD simulations of electrochemical interfaces and proposed a crude road map of what future calculations could contribute to understanding technology. As an example of current simulation capability we discussed the structure of electric double layers for systems with 1500 water molecules and salt concentrations from 1M to 3M NaCl. Water structure near charged metal walls is not an artifact of small size. In 1M NaCl the double layer is about 1 nm thick (about three layers of water) while in 3M solution the screening layer was narrower than a water molecule. Water layers at the surface significantly affected the distribution of ions near the metal creating features in the probability distributions that are not describable in the Gouy-Chapman-Stern model.

Literature Cited

1. Gileadi, E., Kirowa-Eisner, E., Penciner, J. Addison-Wesley: Reading, Massachusetts, 1975.
2. Grahame., D. C. *Chem. Rev.* **1947**, *41*, 441 - 501.
3. Brockris, J. O., Devanathan, M. A., Müller, K. *Proc. Roy. Soc.(London)* **1963.**, *A274*, 55-79.
4. Dutkiewicz, E., Parsons, R. *J. Electroanal. Chem.* **1966**, *11*, 100.
5. Parsons, R. *Chem. Rev.* **1990**, *90*, 813-826.
6. Hautman, J., Halley, J. W., Rhee, Y. *J. Chem. Phys.* **1989**, *91*, 467-472.
7. Rhee, Y. J., Halley, J. W., Hautman, J., Rahman, A. *Phys. Rev. B* **1989**, *40*, 36-42.
8. Born, M., Huang, K. The Clarendon Press: Oxford, England, 1954.
9. Schacher, G. E., de Wette, F. W. *Phys. Rev.* **1965**, *136A*, 78-91.
10. Greengard, L. F. The MIT Press: Cambridge, Massachusetts, 1987.
11. Greengard, L., Rokhlin, V. *J. Comp. Phys.* **1987**, *73*, 325-348.
12. Carrier, J., Greengard, L., Rokhlin, V. *Siam J. Sci. Stat. Comput.* **1988**, *9*, 669-686.
13. Greengard, L., Rokhlin, V. *Chemica Scripta* **1989**, *29A*, 139-144.
14. Glosli, J. N., Philpott, M. R. In *Symposium on Microscopic Models of Electrode-Electrolyte Interfaces. Symp. Proc. 93-5*; J. W. Halley L. Blum, Ed.; Electrochem. Soc.: Pennington, New Jersey, 1993. 80-90.
15. Hockney, R. W., Eastwood, J. W. McGraw-Hill: New York, 1981.
16. Pollock, R., Glosli, J. N. *J. Comp. Phys.* **1996**.
17. Glosli, J. N., Philpott, M. R. *Electrochemica Acta* **1996**, *41*.
18. Philpott, M. R., Glosli, J. N. *J. Electroanal. Chem.* **1996**.
19. Halley, J. W., Hauptman, J. *Phys. Rev. B* **1988**, *38*, 11704-11710.
20. Philpott, M. R., Glosli, J. N., Roberts, J. *unpublished* **1996**.
21. Stone, A. J. *Molec. Phys.* **1985**, *56*, 1065 - 1082.
22. Price, S. L. *Phil. Mag.* **1994**.

23. Dang, L. X., Caldwell, J., Kollman, P. A. **1990**.
24. Barker, J. A., Rettner, C. T. *J. Chem. Phys.* **1992**, *97*, 5844 - 5850.
25. Zhu, S., Philpott, M. R. *J. Chem. Phys.* **1994**, *100*, 6961-6968.
26. Pacchioni, G., Bagus, P. S., Nelin, C. J., Philpott, M. R. *Internat. J. Quantum Chem.* **1990**, *38*, 675-689.
27. Heinzinger, K. In *Computer Modeling of Fluids Polymers and Solids,*; C. R. A. Catlow, S. C. Parker, M. P. Allen, Ed.; Kluwer, Holland: 1990;
    293, NATO ASI Series C. 357-404.
28. Reddy, M. R., Berkowitz, M. *Chem. Phys. Letters* **1989**, *155*, 173-176.
29. Raghavan, K., Foster, K., Motakabbir, K., Berkowitz, M. *J. Chem. Phys.* **1991**, *94*, 2110-2117.
30. Sellers, H., Sudhakar, P. V. *J. Chem. Phys.* **1992**, *97*, 6644 - 6648.
31. Nazmutdinov, R. R., Probst, M. M., Heinzinger, K. *J. Electroanal. Chem.* **1994**, *369*, 227 - 231.
32. Spohr, E. *Chem. Phys.* **1990**, *141*, 87 - 94.
33. Rose, D. A., Benjamin, I. *J. Chem. Phys.* **1991**, *95*, 6856-6865.
34. Perera, L., Berkowitz, M. L. *J. Phys. Chem.* **1993**, *97*, 13803 - 13806.
35. Car, R., Parrinello, M. *Phys. Rev. Lett.* **1985**, *55*, 2471.
36. Löwen, H., Hansen, J., Madden, P. A. *J. Chem. Phys.* **1993**, *98*, 3275-3289.
37. Straus, J. B., Voth, G. A. *J. Phys. Chem.* **1993**, *97*, 7388-7391.
38. Marcus, R. M. *J. Chem. Phys.* **1965**, *43*, 679.
39. Halley, J. W., Hautman, J. *Ber. Bunsenges. Phys. Chem.* **1987**, *91*, 491-496.
40. Bader, J. S., Chandler, D. *J. Phys. Chem.* **1992**, *96*, 6423 - 6427.
41. Bennett, C. H. In *Algorithms for Chemical Computations*; R. E. Christoffersen, Ed.; ACS Symposium Series 46: Washington DC, 1977. 63-97.
42. Andersen, H. C. *J. Chem. Phys.* **1980**, *72*, 2384.
43. Smit, B. In *Computer Simulation in Chemical Physics,*; M. P. Allen D. J. Tildesley, Ed.; Kluwer, Holland: 1993;
    397, NATO ASI Series C. 173-209.
44. Nicholson, D., Parsonage, N. G. Academic Press: New York, 1982.
45. Cracknell, R. F., Nicholson, D., Quirke, N. *Mol. Phys.* **1993**, *80*, 885 - 897.
46. Laasonen, K., Sprik, M., Parrinello, M., Car, R. *preprint* **1993**.
47. Tuckermann, M., Laasonen, K., Sprik, M., Parrinello, M. *preprint* **1994**.
48. Brenner, D. W. *Phys. Rev. B* **1990**, *42*, 9458-9471.
49. DePristo, A. E., Kara, A. *Adv. Chem. Phys.* **1990**, *77*, 163 - 253.
50. Brenner, D. W., Garrison, B. J. *Phys. Rev. B* **1985**, *34*, 1304.
51. Stillinger, F. H., David, C. W. *J. Chem. Phys.* **1978**, *69*, 1473-1484.
52. Halley, J. W., Rustad, J. R., Rahman, A. *J. Chem. Phys.* **1993**, *98*, 2435-2438.
53. Glosli, J. N., Philpott, M. R. In *Microscopic Models of Electrode-Electrolyte Interfaces. Symp. Proc. 93-5*; J. W. Halley L. Blum, Ed.; Electrochem. Soc.: Pennington, New Jersey, 1993. 90-103.
54. Philpott, M. R., Glosli, J. N. In *Theoretical and Computational Approaches to Interface Phenomena*; H. Sellers J. T. Golab, Ed.; Plenum: New York, 1994. 75 - 100.
55. Glosli, J. N., Philpott, M. R. *J. Chem. Phys.* **1992**, *96*, 6962-6969.

56. Glosli, J. N., Philpott, M. R. *J. Chem. Phys.* **1993**, *98*, 9995-10008.

57. Berendsen, H. J., Grigera, J. R., Straatsma, T. P. *J. Chem. Phys.* **1987**, *90*, 6267.

58. Impey, R. W., Madden, P. A., McDonald, I. R. *J. Phys. Chem.* **1983**, *87*, 5071 - 5083.

59. Lee, C. Y., McCammon, J. A., Rossky, P. J. *J. Chem. Phys.* **1984**, *80*, 4448-4455.

60. Goodisman, J. Wiley-Interscience: New York, 1987.

61. Gouy, G. *Ann. phys.* **1917**, *7*, 129.

62. Chapman, D. L. *Phil. Mag.* **1913**, *25*, 475.

63. Bockris, J. O., Reddy, A. K. Plenum Press: New York, 1973; 1.

64. Conway, B. E., Bockris, J. O., Ammar, I. A. *Trans. Faraday Soc.* **1951**, *47*, 756 - 766.

65. Landau, L. D., Lifschitz, E. M. Addison-Welsey: 1960; 99 - 101.

66. Samec, Z., Johnson, B. W., Doblhofer, K. *Surface Sci.* **1992**, *264*, 440 - 448.

67. Stuve, E. M., Kizhakevariam, N. *Surface Sci.* **1993**, *A 11*, 2217 - 2224.

68. Wilson, M. A., Pohorille, A., Pratt, L. R. *J. Chem. Phys.* **1988**, *88*, 3281 - 3285.

69. Wilson, M. A., Pohorille, A., Pratt, L. R. *Chem. Phys.* **1989**, *129*, 209 - 212.

70. Wilson, M. A., Pohorille, A., Pratt, L. R. *J. Chem. Phys.* **1989**, *90*, 5211 - 5213.

71. Philpott, M. R., Glosli, J. N., Zhu, S. *unpublished* **1996**.